Ground-state properties of a quasi-one-dimensional electron gas within a dynamical self-consistent mean-field approximation

Vinayak Garg,[1,2] R. K. Moudgil,[2,*] Krishan Kumar,[2] and P. K. Ahluwalia[1]
[1]*Department of Physics, Himachal Pradesh University, Shimla 171 005, India*
[2]*Department of Physics, Kurukshetra University, Kurukshetra 136 119, India*
(Received 24 December 2007; revised manuscript received 23 May 2008; published 3 July 2008)

The ground-state properties of the quasi-one-dimensional electron gas are determined theoretically within the quantum/dynamical version of the self-consistent mean-field approximation of Singwi, Tosi, Land, and Sjölander (the so-called qSTLS approach). The transverse motion of electrons is assumed to be confined by a harmonic potential. The calculated static structure factor, pair-correlation function, and correlation energy are compared directly with the recent findings of lattice regularized diffusion Monte Carlo simulation study due to Casula *et al.* It has been found that the qSTLS results are overall in better agreement with the simulation data than the predictions based upon static mean-field theories. Results for the dynamic local-field correction, dynamic structure factor, and plasmon excitation energy are also reported. The qSTLS approach is found to yield an inadequate description of the dynamic properties; for instance, the dynamic structure factor was seen to become negative over a range of frequencies. Our theoretical predictions, seen in conjunction with similar studies on the three- and two-dimensional electron systems, lead us to conclude that the correlation effects are relatively more pronounced in one-dimensional electron gas.

DOI: 10.1103/PhysRevB.78.045406 PACS number(s): 73.21.Hb, 71.45.Gm, 73.20.Qt

I. INTRODUCTION

The quasi-one-dimensional electron gas (Q1DEG) constitutes a basic theoretical model[1–5] to describe the physical behavior of quasi-one-dimensional (Q1D) electron systems. Such systems exist, for instance, in high-mobility semiconductor quantum wires.[6,7] Here, electrons have a quasi-free motion along the length of the wire while their motion is restricted quantum-mechanically along the transverse directions by means of confining potential. These systems are found to exhibit a variety of interesting physical phenomena such as fractionalized conductance,[8,9] enhancement in Wigner crystallization,[9,10] etc. Quite generally, the restricted dynamics of electrons in one-dimension would cause the interaction effects to become relatively more pronounced over the kinetic effects as compared to higher dimensional situations. There have been studies[9,11,12] indicating that the confined dynamics in an exceptionally clean 1D electron system may favor the Tomonaga–Luttinger liquid[13] behavior rather than the usual Fermi-liquid description. However, Hu and Das Sarma[14] have argued that even the slightest amount of impurity and/or finite temperature may restore the Fermi-liquid behavior of the 1D electron system. Even though we are not considering here the effects pertaining to disorder and finite temperature, we shall employ a Fermi-liquid description of 1D electrons. In this paper, we are interested in the theoretical study of the ground-state behavior of such a Q1DEG.

Recently, Casula *et al.*[15] have studied the ground-state properties of the Q1DEG with a harmonic transversal potential by using the lattice regularized diffusion Monte Carlo (LRDMC) simulation technique. The exact correlation energy has been calculated over a wide range of electron number density and wire width. In addition, the static density correlation functions (both in the Fourier and real spaces) have also been reported. Apart from having other applications, the LRDMC calculation has provided a benchmark for testing the accuracy/validity of the predictions of different approximate many-body theories. However, no such comparison with the LRDMC data has appeared so far and this forms a part of our motivation for the present study on Q1DEG. Earlier, Das Sarma and co-workers[2,16,17] applied the random-phase approximation (RPA) to obtain the ground-state behavior of Q1DEG. But, the RPA neglects completely the short-range correlations among electrons, which are otherwise believed to become even more pronounced in reduced dimensions. Therefore, except at relatively high electron density and/or large wire width (i.e, weak-coupling regime), the RPA is not expected to provide an accurate description of many-body properties. Correlations beyond RPA have been included by Calmels and Gold[3,18,19] through a static local-field correction (LFC) factor determined by using the different versions of the so-called sum-rule approach (SRA). It has been shown that correlation effects become increasingly dominant with decreasing density and/or wire width. It may be mentioned here that the SRA is based upon the self-consistent mean-field approximation of Singwi, Tosi, Land, and Sjölander (STLS),[20] and has the advantage that the LFC factor can be obtained analytically. Correlation effects in Q1DEG have also been studied by using the Ladder[21,22] and STLS (Ref. 22) approximations.

Authors in Ref. 15 have also compared their LRDMC results of correlation energy with the predictions of the three-sum-rule approach (3SRA) (Ref. 19) and the agreement was seen to be reasonable only in the weak-coupling domain. Besides other reasons, this might be due to the fact that the correlations were treated as time independent in the 3SRA. However, the dynamics of correlations is known[23–25] to become crucial in the intermediate-strong-coupling domain and this aspect of correlations is expected to become even more significant in 1D than the higher dimensional situations due to increased dominance of the interaction effects in low di-

 ©2008 The American Physical Society

mensions. Therefore, the aim of the present work is to provide a self-contained theoretical study of the ground-state properties of Q1DEG by incorporating the dynamics of correlations. To enable a direct comparison of our results with simulation data, we shall employ here the same wire model as that used by Casula *et al.*[15] in their LRDMC study. For dealing with the dynamics of correlations, we shall make use of the quantum version of the self-consistent mean-field approximation of Singwi, Tosi, Land, and Sjölander (qSTLS).[26] In this approach, the correlations enter in the form of a LFC factor to the bare Coulomb potential, and as an important improvement over the original STLS method,[20] the LFC factor is frequency dependent. Tanatar and Bulutay[27] have earlier used the qSTLS method in 1D but for a different confinement model. Thus, one cannot compare their predictions with the LRDMC study and, hence, comment on the quality of their results.

The paper is organized as follows: In Sec. II, we describe the quantum wire model and theoretical formalism. Results and discussion are given in Sec. III. Summary and conclusions are presented in Sec. IV.

II. WIRE MODEL AND THEORETICAL FORMALISM

A. Wire model

We consider an electron quantum wire, in which electrons are assumed to be embedded in a rigid positive charge neutralizing background. A lateral confinement is provided to electrons by means of a harmonic transversal potential, $V_c(r_\perp)=\hbar^2 r_\perp^2/(8m^* b^4)$. Here, m^* is the effective mass of the electrons and b is the width of the wire. Evidently, b tunes the strength of the confinement potential. The confinement is assumed to be sufficiently strong so that the electrons occupy only the lowest energy subband in the confinement direction. At absolute zero, the system is characterized completely by the dimensionless density parameter r_s and the wire width b. r_s is related to linear electron number density n as $r_s=1/(2na_0^*)$ while $a_0^*=\epsilon_0\hbar^2/(m^*e^2)$ is the effective Bohr atomic radius, with ϵ_0 being the background dielectric constant. The electrons in the wire interact via a (long-range) Coulomb potential. In the lowest energy subband, the Fourier transform of the interaction potential is given as

$$V(q)=\frac{e^2}{2\epsilon_0}f(qb), \tag{1}$$

with

$$f(x)=2E_1(x^2)\exp(x^2).$$

Here, $E_1(x)$ is the exponential-integral function. For $x\gg 1$, $f(x)\approx 2/x^2$ and for $x\ll 1$, $f(x)\approx 4\ln|1/x|$. These limiting forms of $f(x)$ are quite useful in the numerical work.

It can be shown that the single subband approximation is justified for $r_s > \pi b/(4a_0^*)$, which implies that the intersubband energy difference in the electron quantum wire remains larger than the Fermi energy.

In this work, we also assume that the number of electrons with up spin is exactly equal to the number of electrons with down spin, i.e., $N_\uparrow=N_\downarrow=N/2$ (N being the total number of electrons), and therefore, the system under consideration has zero net spin polarization. This assumption is made since the Lieb–Mattis theorem[28] states that the 1D electron system remains in the paramagnetic ground state at all electron densities.

B. Theoretical formalism

We use the dielectric formulation where the Q1DEG is subjected to a weak space-time dependent external longitudinal electric potential. Here, the dynamic density response function $\chi(q,\omega)$, which describes the density response of the electron system, constitutes a quantity of central importance. All the relevant ground-state properties of the system can be obtained from the knowledge of $\chi(q,\omega)$. An exact calculation of $\chi(q,\omega)$ is not feasible. However, considerable progress has been made in literature to develop approximate many-body theories to determine $\chi(q,\omega)$. In our study, we make use of the dynamical self-consistent mean-field approximation, where $\chi(q,\omega)$ is given as

$$\chi(q,\omega)=\frac{\chi_0(q,\omega)}{1-V(q)[1-G(q,\omega)]\chi_0(q,\omega)}. \tag{2}$$

In the above equation, $\chi_0(q,\omega)$ is the density response function of the noninteracting electron system and $G(q,\omega)$ is the dynamic LFC factor, which accounts for the short-range correlations among electrons. We determine $G(q,\omega)$ by using the nonperturbative scheme of Hasegawa and Shimizu originally developed for the 3DEG.[26] This scheme is commonly referred to as the qSTLS approach as it is based upon the pioneering work of Singwi, Tosi, Land, and Sjölander[20] except for the difference that Hasegawa and Shimizu replaced the classical distribution function with its quantum counterpart. For Q1DEG, $G(q,\omega)$ in the qSTLS approach is given as

$$G(q,\omega)=-\frac{1}{n}\int_{-\infty}^{\infty}\frac{dq'}{2\pi}\frac{\chi_0(q,q',\omega)V(q')}{\chi_0(q,\omega)V(q)}[S(q-q')-1]. \tag{3}$$

$\chi_0(q,q',\omega)$ is the inhomogeneous density response function of the noninteracting Q1DEG and is given by

$$\chi_0(q,q',\omega)=-\frac{2}{\hbar}\int_{-\infty}^{\infty}\frac{dp}{h}\frac{f_0(p+\hbar q'/2)-f_0(p-\hbar q'/2)}{\omega-pq/m^*+\iota\eta}. \tag{4}$$

Here, $f_0(p)$ is the usual equilibrium Fermi–Dirac distribution function. It may be noted that $\chi_0(q,q',\omega)$ reduces to $\chi_0(q,\omega)$ for $q'=q$. The static structure factor $S(q)$ in Eq. (3) is related to the imaginary part of $\chi(q,\omega)$ through the fluctuation-dissipation theorem as,[29]

$$S(q)=-\frac{\hbar}{\pi n}\int_0^{\infty}d\omega \mathrm{Im}\chi(q,\omega). \tag{5}$$

Evidently, the density response function $\chi(q,\omega)$ can only be obtained numerically from the self-consistent solution of Eqs. (2), (3), and (5). Other relevant ground-state properties follow directly from the knowledge of $\chi(q,\omega)$.

The pair-correlation function $g(r)$, which represents the probability of finding an electron at a distance r away from another electron at origin, can be obtained from the inverse Fourier transform of $S(q)$ as

$$g(r) = 1 + \frac{1}{n}\int_{-\infty}^{\infty} \frac{dq}{2\pi} e^{-\iota qr}[S(q) - 1]. \tag{6}$$

The ground-state energy E_g (per particle) of the Q1DEG can be obtained by using the ground-state energy theorem as[30]

$$E_g = \frac{p_F^2}{6m^*} + \int_0^{e^2} d\lambda \frac{E_{\rm int}(\lambda)}{\lambda}, \tag{7}$$

where the first term is the kinetic-energy contribution while the second term represents the potential energy with

$$E_{\rm int}(\lambda) = \int_0^{\infty} \frac{dq}{2\pi} V(q,\lambda)[S(q,\lambda) - 1]. \tag{8}$$

Here, λ is the usual coupling constant and $S(q,\lambda)$ is the static structure factor of Q1DEG, having coupling λ.

We should point out in passing that in the limit $\hbar \to 0$, the qSTLS LFC factor $G(q,\omega)$ [Eq. (3)] reduces to

$$G(q) = -\frac{1}{n}\int_{-\infty}^{\infty} \frac{dq'}{2\pi} \frac{q'V(q')}{qV(q)}[S(q-q') - 1], \tag{9}$$

which is simply the LFC factor of the original STLS approach.

In the next section, we present numerical results for various ground-state properties of Q1DEG.

III. RESULTS AND DISCUSSION

A. Static properties

In numerical calculations and results presented, we take q in units of the Fermi wave vector k_F, wire width b in the effective Bohr atomic radius a_0^*, and energies in the effective Rydberg [$1\text{Ry}d^* = e^2/(2\epsilon_0 a_0^*)$].

The set of Eqs. (2), (3), and (5) are solved numerically in a self-consistent manner. To avoid the numerical problem of dealing with the plasmon poles on the real frequency axis, we transform the ω integral in Eq. (5) to the imaginary frequency axis through Wick's rotation. Consequently, Eq. (5) takes the form

$$S(q) = -\frac{\hbar}{\pi n}\int_0^{\infty} d\omega \chi(q,\iota\omega). \tag{10}$$

An explicit expression of $\chi_0(q,q',\omega)$ on both the real and imaginary frequency axes is given in Appendix A.

We accepted the numerical solution when convergence in the results of $S(q)$ was better than 0.0001% at each q in the grid of q points. However, we could generate in this way the self-consistent $S(q)$ only for $r_s < r_s^c$ with r_s^c found to be an increasing function of b. For $r_s \geq r_s^c$, it became almost impossible to find the self-consistent $S(q)$. Tanatar and Bulutay[27] have also reported a similar kind of numerical problem in their study of Q1DEG. Looking carefully into the different steps involved in the calculation of $S(q)$, we resolve that this problem originates from the fact that there starts appearing, during the iterative calculation, a numerical instability in $S(q)$ while performing the ω integration in Eq. (10). In particular, for $r_s \geq r_s^c$, $\chi(q,\iota\omega)$ starts exhibiting over a range of q values (say, $q_{c1} \leq q \leq q_{c2}$) a pole at a finite frequency, say $\omega_0(q)$. Moreover, in the limit $r_s \to r_s^c$, the width of q interval (i.e., $\{q_{c2} - q_{c1}\}$) as well as $\omega_0(q)$ tend to zero. Since the ω integration in Eq. (10) is being performed along the imaginary ω axis, the appearance of a pole in $\chi(q,\iota\omega)$ obviously constitutes an unphysical result as such a pole corresponds to an excitation of the electron system at an imaginary frequency. Nevertheless, it would be interesting to handle this pole in $\chi(q,\iota\omega)$ in a purely mathematical sense, and explore its effect on the behavior of $S(q)$ and other ground-state properties of the electron system. Allowing for the existence of a pole at $\omega = \omega_0(q)$ on the imaginary ω axis, the Eq. (10) gets modified[31] as (for details, see Appendix B)

$$S(q) = -\frac{\hbar}{\pi n}\int_0^{\infty} d\omega \left[\chi(q,\iota\omega) - \frac{a_{-1}}{\omega - \omega_0(q)} + \frac{a_{-1}}{\omega + \omega_0(q)}\right], \tag{11}$$

where a_{-1} is the residue of $\chi(q,\iota\omega)$ at $\omega = \omega_0(q)$. Using the above expression of $S(q)$, we were able to obtain the self-consistent $S(q)$ for $r_s \geq r_s^c$. However, the number of iterations required to achieve self-consistent solution increases. It may be pointed out that the poles of $\chi(q,\iota\omega)$, if any, are to be located numerically.

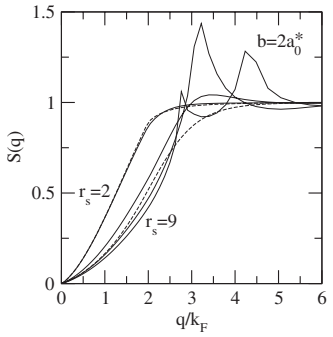

FIG. 1. Static structure factor $S(q)$ are plotted as a function of q/k_F at $b = 2a_0^*$ in the qSTLS (solid lines) for $r_s = 2$, 5, 7.5, and 9, and STLS (dashed lines) for $r_s = 2$ and 7.5.

In Fig. 1, we plot the static structure factor $S(q)$ for different values of r_s at wire width $b = 2a_0^*$. For comparison, the STLS results are also shown at selected values of r_s. We observe that $S(q)$ begins exhibiting a peak at q around $3.4k_F$ for $r_s \geq 5$ and its magnitude grows with further increase in r_s. The peak height is seen to be maximum at $r_s = r_s^c \approx 7.5$; one may recall here that r_s^c is the critical density at which pole appears in $\chi(q,\iota\omega)$ for the first time. For r_s above r_s^c, a double-peak structure starts appearing in $S(q)$. This point is illustrated in Fig. 1 by showing $S(q)$ at $r_s = 9$. We find that the locations of the two peaks depend upon r_s and their mutual separation increases with increasing r_s. It is interesting to note that the appearance of two-peak structure in $S(q)$ is

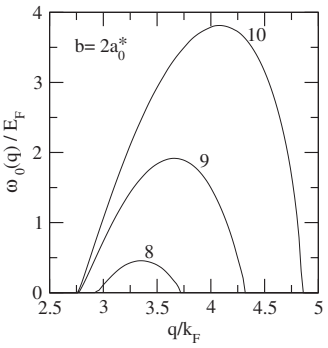

FIG. 2. Position of the pole $\omega_0(q)/E_F$ [which appears in $\chi(q,\iota\omega)$ for $r_s \geq r_s^c$] are plotted as a function of q/k_F at $b=2a_0^*$. E_F is the Fermi energy. Legends indicate the values of r_s.

directly related to the emergence of poles in $\chi(q,\iota\omega)$. In particular, we find that the positions of the two peaks in $S(q)$ correspond, respectively, to the lowest (i.e., q_{c1}) and the highest (i.e., q_{c2}) values of q in the q interval, over which $\chi(q,\iota\omega)$ has poles. For the sake of further clarity, we have illustrated in Fig. 2 the r_s dependence of $\omega_0(q)$ at $b=2a_0^*$. It is apparent that $\omega_0(q)$ is a smooth function of q. With increasing r_s, the q interval is seen to broaden in a monotonic way. However, we must mention here that the qSTLS predictions of the ground-state properties are not reliable for $r_s > r_s^c$ due to the appearance of unphysical poles in $\chi(q,\iota\omega)$ at finite ω.

A similar qualitative behavior of $S(q)$ is found at other values of wire width. In particular, we show in Fig. 3 the results of $S(q)$ at $b=0.1a_0^*$ for different r_s, where the LRDMC simulation data is available to draw a direct comparison. The STLS results are also given in the same figure. It is worthwhile to mention here that $\chi(q,\iota\omega)$ exhibits pole for the first time at $r_s=r_s^c \approx 3$ for $b=0.1a_0^*$. From Fig. 3, we notice that the qSTLS curves are overall in better agreement with the simulation data. Notably, the qSTLS theory accounts for $r_s > 1$, at least at the qualitative level, for the peaked structure of the LRDMC $S(q)$, which otherwise is completely missing in the predictions of the STLS approximation. However, the qSTLS theory underestimates the peak height in $S(q)$ and, in fact, the qSTLS curve at $r_s=3$ is seen to resemble closely the LRDMC data at $r_s=2$. Also, in sharp contrast with the LRDMC $S(q)$ (although not shown here), the qSTLS predicts

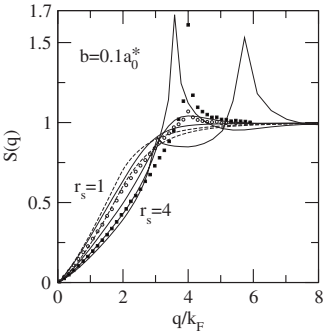

FIG. 3. Static structure factor $S(q)$ are plotted as a function of q/k_F at $b=0.1a_0^*$ in the qSTLS (solid lines) for $r_s=1$, 2, 3, and 4, and STLS (dashed lines) for $r_s=1$ and 2. Symbols represent the LRDMC data for $r_s=1$ (open circles) and 2 (solid squares).

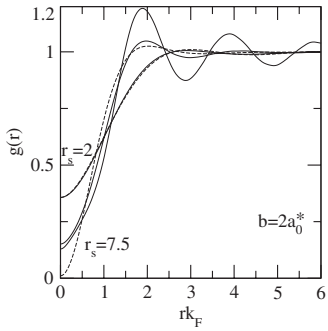

FIG. 4. Pair-correlation function $g(r)$ at $b=2a_0^*$ in the qSTLS (solid lines) for $r_s=2$, 5, and 7.5, and STLS (dashed lines) for $r_s=2$ and 7.5.

a double-peak structure in $S(q)$ at $r_s=4$. Recalling the relation of the two-peak structure in $S(q)$ with the emergence of unphysical poles in $\chi(q,\iota\omega)$ at finite ω, the qualitative mismatch between the qSTLS $S(q)$ and the LRDMC data at $r_s=4$ further highlights the breakdown of the qSTLS approach for $r_s > r_s^c$. Nevertheless, our results seem to provide some insight into the mechanism that leads to the breakdown of qSTLS approach beyond r_s^c.

The proximity of the location ($q/k_F \approx 3.6$) of single strong peak in $S(q)$ to the 1D reciprocal-lattice vector ($q/k_F=4$) and the result that the only pole in $\chi(q,\iota\omega)$ at $r_s=r_s^c$ occurs at q coinciding the peak position in $S(q)$ with $\omega_0(q) \to 0$ signals the evolution of an ordered structure in the electron quantum wire at $r_s=r_s^c$. It is appropriate to mention here that a single strong peak in $S(q)$ was also found earlier by Tanatar and Bulutay[27] for a Q1DEG but for a different confinement model.

In Figs. 4 and 5, we depict the results of pair-correlation function $g(r)$ for selected values of r_s at $b/a_0^*=2$ and 0.1, respectively. To highlight the importance of the dynamical nature of correlations, the STLS results are also shown. On expected lines, the correlations are found to grow in their magnitude with increasing r_s at a given b and with decreasing b at a given r_s. In particular, $g(r)$ starts exhibiting oscillatory behavior as one moves to sufficiently large (small) values of r_s (b) in the qSTLS approach. At $b=0.1a_0^*$, the LRDMC data is available and it is shown by symbols in Fig.

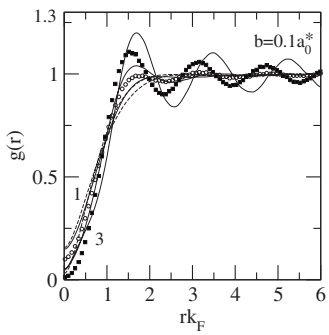

FIG. 5. Pair-correlation function $g(r)$ at $b=0.1a_0^*$ in the qSTLS (solid lines) for $r_s=1$, 2, and 3, and STLS (dashed lines) for $r_s=1$ and 2. Symbols represent the LRDMC data for $r_s=1$ (open circles) and 2 (solid squares). Legends indicate the values of r_s.

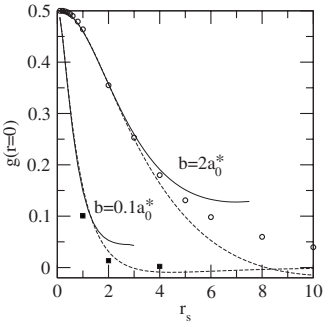

FIG. 6. Contact pair-correlation function $g(r=0)$ as a function of r_s at $b/a_0^*=2$ and 0.1 in the qSTLS (solid lines) and STLS (dashed lines) approaches. Solid squares and open circles represent, respectively, the LRDMC and the Ladder theory results. The qSTLS curves are plotted for $r_s \leq r_s^c$.

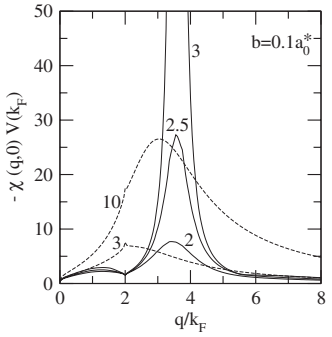

FIG. 7. Static density susceptibility $\chi(q,0)$ are plotted as a function of q/k_F at $b=0.1a_0^*$ in qSTLS approach (solid lines) for the indicated values of r_s. For comparison, STLS results (dashed lines) are also depicted at $r_s=3$ and 10.

5. One may note that the emergence of oscillatory trend in $g(r)$ in qSTLS is in qualitative agreement with the LRDMC study. On the other hand, the STLS curves of $g(r)$ do not contain any sort of oscillatory structure. The dominant periodic oscillations in the qSTLS $g(r)$ at $r_s=r_s^c$ constitute a precursor for the onset of an ordered phase in Q1D electron system.

In Fig. 6, we illustrate specifically the behavior of short-range correlations by plotting the contact pair-correlation function $g(r=0)$ as a function of r_s at $b/a_0^*=2$ and 0.1. The apparent departure of $g(r=0)$ from its corresponding Hartree–Fock value (i.e., 0.5) is a direct manifestation of Coulomb correlation among electrons and our results reveal that these correlations grow strongly with the decreasing density (wire width) at a given wire width (density). Wherever available, we have also compared our results with the LRDMC data and the Ladder theory predictions from Calmels and Gold.[21] At $b=2a_0^*$, both the qSTLS and STLS curves almost overlap with the results of Ladder theory in the weak-coupling domain while there appears a noticeable difference at large r_s values. For $b=0.1a_0^*$, our results are reasonably close to the LRDMC data and the Ladder theory results are not available for comparison.

To explore further the behavior of Q1DEG in the strong-coupling regime, we determine the static density susceptibility $\chi(q,0)$, which can be obtained from Eq. (2), by setting $\omega=0$ as

$$\chi(q,0) = \frac{\chi_0(q,0)}{1 - V(q)[1 - G(q,0)]\chi_0(q,0)}. \tag{12}$$

Evidently, the calculation of $\chi(q,0)$ requires $\chi_0(q,0)$ and self-consistent static LFC factor $G(q,0)$. Using Eq. (3), $G(q,0)$ can be obtained in a straightforward manner from the knowledge of self-consistent $S(q)$. Results of $\chi(q,0)$ for relevant values of r_s are given in Fig. 7 at $b=0.1a_0^*$. Quite generally, $\chi(q,0)$ has a well-defined peak at $q \approx 3.6k_F$ and the peak-height is found to grow monotonically with increasing r_s. This peak is eventually found to diverge at $r_s=3$. The presence of a diverging peak in $\chi(q,0)$ at $q \approx 3.6k_F$ signals the occurrence of a structural phase transition in Q1D electron system from the liquid phase to the Wigner crystal (WC) state at $r_s=3$. The onset of Wigner crystallization also reflects in the behavior of $S(q)$ and $g(r)$ (see Figs. 3 and 5). Earlier, density-functional theory based calculation[32] has also predicted the formation of Wigner crystal at sufficiently low densities in the electron quantum wire. At this juncture, we would like to mention that the Mermin–Wagner theorem[33] excludes the existence of a crystalline long-range order in a strictly 1D electron system at any nonzero temperature, provided[34] the interaction potential be integrable at infinity (i.e., $V(r) \sim 1/r^{1+|\epsilon|}$ at large r with ϵ arbitrarily small), and repulsive and nonintegrable for $r \to 0$. In our 1DEG model $V(r) \sim 1/r$ and $T=0$ K, and therefore, it is not obvious whether the Mermin–Wagner theorem be directly applicable. However, Schulz[12] has shown, using the bosonization approach, that at absolute zero the long-range nature of the Coulomb force in a 1D electron gas, even if it is arbitrarily weak, gives rise to the formation of a quasi-Wigner crystal state. The LRDMC simulations have also indicated the possibility of a quasi-Wigner crystal phase at $r_s \approx 4$ for $b=0.1a_0^*$. Therefore, the qSTLS prediction on Wigner crystallization in 1D may be an artifact of the misrepresentation of correlations in the strongly correlated region.

We have also investigated the STLS $\chi(q,0)$ and found that it does not exhibit any singularity; for instance, the STLS results of $\chi(q,0)$ are reported in Fig. 7 for $r_s=3$ and 10 at $b=0.1a_0^*$. This obviously points to a different behavior of the static LFC factor in the qSTLS and STLS approaches. We illustrate this in Fig. 8 by plotting the qSTLS $G(q,0)$ and the STLS $G(q)$ for $r_s=2$, 2.5, and 3 at $b=0.1a_0^*$. It is noticed that $G(q,0)$ exhibits an oscillatory behavior with clear maxima and minima, and, at large q, it approaches $[1-g(r=0)]$. The maximum value of $G(q,0)$ at $q \approx 4k_F$ lies well above unity, thus causing the corresponding effective interaction potential, i.e., $\{V(q)[1-G(q,0)]\}$, to become attractive. It is this character of $G(q,0)$ that is solely responsible for the singular behavior of $\chi(q,0)$, and hence, for the transition from liquid to the WC state in Q1D system. Another peculiar feature of the 1D $G(q,0)$ is that it becomes exactly zero at $q=2k_F$ for all r_s and b due to a logarithmic singularity in $\chi_0(q,0)$. This type of behavior of $G(q,0)$ was also noticed by Nagano and Singwi[35] in their investigation of 1D fermions interacting via a repulsive δ-function potential. On the other hand, the STLS $G(q)$ remains always a smooth func-

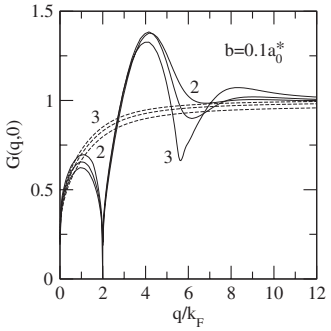

FIG. 8. Comparison between $G(q,0)$ (solid lines) and the STLS $G(q)$ (dashed lines) for $r_s=2$, 2.5, and 3 at $b=0.1a_0^*$.

tion of q, and at large q, it saturates to the value $[1-g(r=0)]$. Accordingly, the STLS $\chi(q,0)$ does not contain any singularity. But, this should not mean that the correlations be treated in a static manner. Furthermore, contrary to the result of the authors in Ref. 27, our $G(q,0)$ remains positive in the liquid density regime. It seems that the negative value of $G(q,0)$ obtained in Ref. 27 is due to the inclusion of disorder effects.

Apart from $G(q,0)$, it is interesting to investigate the behavior of $G(q,\infty)$ for one can easily show that for fixed q, $\lim_{\omega\to\infty} G(q,\omega)=G(q)+\mathcal{O}(1/\omega^2)$, where $G(q)$ is the STLS-type LFC factor given by Eq. (9). This limit implies that the STLS approach is just the large-frequency limit of the qSTLS theory. Figure 9 presents a comparison between $G(q,\infty)$ and the STLS $G(q)$ at $b=2a_0^*$. $G(q,\infty)$ deviates from $G(q)$ at large q and the deviation is seen to build up with increasing r_s. In particular, $G(q,\infty)$ develops a mild peak at q around $3k_F$ for $r_s>5$. The difference in results arises due to the different inputs for the self-consistent $S(q)$ in the two approaches and this fairly represents the importance of the dynamics of correlations in determining even the behavior of the LFC factor at short times.

B. Ground-state energy and correlation energy

To calculate the ground-state energy of the Q1D electron system, we employ the coupling-constant integration method.[30] From Eq. (7), the ground-state energy (per electron) in reduced units is obtained as

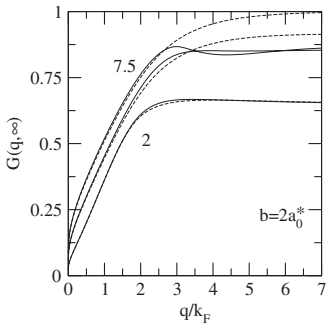

FIG. 9. Comparison between $G(q,\infty)$ (solid lines) and the STLS $G(q)$ (dashed lines) for $r_s=2$, 5, and 7.5 at $b=2a_0^*$.

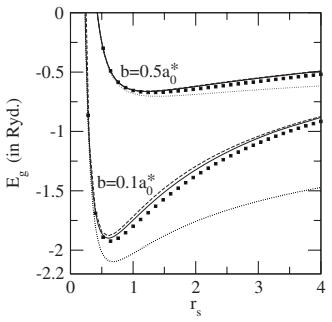

FIG. 10. Ground-state energy E_g (per electron) as a function of r_s in qSTLS (solid lines), STLS (dashed lines), and RPA (dotted lines) at indicated values of wire width. Symbols represent the LRDMC data.

$$E_g=\frac{\pi^2}{48r_s^2}+\frac{k_Fa_0^*}{\pi}\int_0^1 d\lambda\int_0^\infty dq f(bq)[S(q,\lambda e^2)-1]. \tag{13}$$

The correlation energy E_c is the improvement in the ground-state energy of the many-body system over the Hartree–Fock estimate and can be obtained by subtracting the Hartree–Fock ground-state energy E_{HF} from the above equation. In turn, E_{HF} is determined by using the Hartree–Fock $S(q)$ in Eq. (13) as

$$E_{HF}=\frac{\pi^2}{48r_s^2}+\frac{k_Fa_0^*}{\pi}\int_0^2 dq f(bq)[q/2-1], \tag{14}$$

where the second term represents the exchange energy.

In order to calculate the ground-state energy at a given r_s and b, Eqs. (2), (3), and (5) are solved numerically in a self-consistent way to obtain $S(q,\lambda e^2)$ for $0\le\lambda\le1$. It is important to mention here that we have performed integration over the coupling-constant λ and not over the electron-density parameter r_s. In Fig. 10, we report the ground-state energy as a function of r_s at $b/a_0^*=0.5$ and 0.1 in the qSTLS, STLS, and RPA. To make a direct comparison, the simulation data is shown by symbols. It may be noted that both the qSTLS and STLS curves lie quite close to the LRDMC results at $b=0.5a_0^*$. However, at $b=0.1a_0^*$, there is a noticeable difference in the predictions of the two approaches and the qSTLS results compare more favorably with the LRDMC study.

The numerical results of correlation energy are shown in Fig. 11 at $b/a_0^*=0.5$, 1, and 2 for $0.01\le r_s\le6$. The LRDMC and 3SRA results are depicted, respectively, by filled and open symbols. We note that the correlation energy calculated by using the qSTLS theory is overall in better agreement with the simulation data, as compared with the predictions of the STLS, 3SRA, and RPA. However, the extent of agreement decreases at relatively large r_s values and the effect becomes increasingly visible with decreasing wire width b, i.e., in the strong-coupling regime. Evidently, the difference between the qSTLS and STLS predictions continuously builds up with reducing wire width. On the other hand, both the STLS and qSTLS theories have been found to reproduce

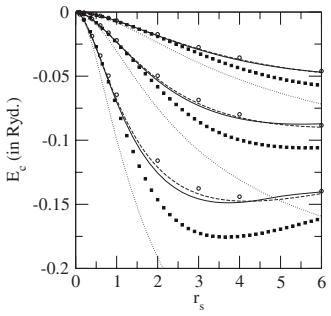

FIG. 11. Correlation energy E_c (per electron) as a function of r_s in qSTLS (solid lines), STLS (dashed lines), and RPA (dotted lines). Curves from top to bottom correspond to $b/a_0^*=2$, 1, and 0.5, respectively. LRDMC and 3SRA results are depicted by filled squares and open circles, respectively.

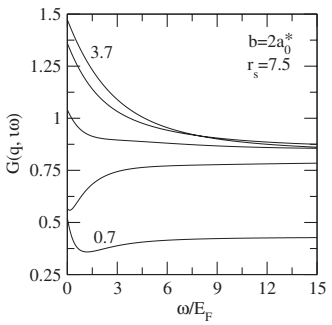

FIG. 12. The dynamic local-field correction factor $G(q,\iota\omega)$ as a function of ω/E_F for $r_s=7.5$ and $b=2a_0^*$. Curves from top to bottom are for $q/k_F=3.7$, 3.2, 2.7, 2.2, and 0.7, respectively.

quite accurately the simulation results of correlation energy for the 3D (Ref. 36) and 2D (Ref. 37) electron systems over a wide range of r_s, including the strongly correlated domain. This seems to reflect the increased dominance of interaction effects with reduction in dimensionality of the electron system. It can also be seen that the RPA, which completely ignores the short-range correlations among electrons, largely overestimates the correlation energy at each wire width. This merely represents the fact that the RPA pair-correlation function $g(r)$ assumes large negative values at small interparticle separation, which directly amounts to an overestimation of the Coulomb hole. Also, we would like to point out here that the STLS results of correlation energy are slightly better than those of the 3SRA calculation due to Calmels and Gold.[19]

In literature, the correlation energy of the Q1DEG has also been calculated[22,27] by using Rice's approach.[38] In view of seemingly less numerical effort involved in these calculations, we have also attempted to determine the correlation energy of the present Q1DEG model by using the expression, as given in Refs. 22 and 27. However, to our surprise, the correlation energy thus obtained does not match with the calculation based upon the method of coupling-constant integration. A thorough analysis of the problem reveals that in the expression of correlation energy employed in Refs. 22 and 27, the integration over the strength of the interaction has been performed analytically. However, this is valid only if the LFC factor is independent of coupling strength; for instance, one can do so in the RPA and Hubbard approximation, and accordingly, the correlation energy in these approximations turns out to be the same as that obtained by using the coupling-constant integration method. The LFC factor, both in the STLS and qSTLS approximations, depends upon the coupling among electrons, and therefore, the integration over coupling-constant cannot be performed analytically here. A similar viewpoint has also been expressed by Schulze *et al.*[39] in case of 2DEG.

C. Dynamic properties

In this section, we start with the discussion of the dynamic LFC factor, which constitutes an important ingredient in the calculation of dynamic properties. The LFC factor is found to exhibit markedly different frequency-dependence along the real and imaginary ω axis. Figure 12 reveals the ω dependence of $G(q,\iota\omega)$ at selected q values for $r_s=7.5$ and $b=2a_0^*$. We note that $G(q,\iota\omega)$ is a smooth function of ω, which justifies the transformation of the frequency integral in Eq. (5) to imaginary ω axis. Most of the frequency dependence in $G(q,\iota\omega)$ is confined to the low-frequency region while it tends to a constant value for large ω at a given q. It may be recalled here that $r_s=7.5$ is the critical r_s for $b=2a_0^*$ at which $\chi(q,\iota\omega)$ exhibits pole for the first time. We now see that this pole originates from the fact that $G(q,\iota\omega)$ lies well above unity at small ω, which in turn makes the denominator of $\chi(q,\iota\omega)$ [see Eq. (2)] to change sign at $q/k_F\approx 3.2$. A similar qualitative behavior of $G(q,\iota\omega)$ is observed for other values of wire width also.

On the real ω axis, $G(q,\omega)$ is a complex quantity, and its real and imaginary parts may be obtained from $G(q,\iota\omega)$ by analytic continuation $\iota\omega\rightarrow\omega+\iota\eta$ in Eq. (3). Their numerical results along the real ω axis at $q/k_F=0.8$ and 3.2 are shown in Figs. 13(a) and 13(b), respectively, by taking $b=2a_0^*$, and $r_s=3$, 7.5, and 9. The r_s and q values are selected to demonstrate any specific change in the behavior of $G(q,\omega)$ in the instability region. Quite generally, we note that both the real and imaginary parts of $G(q,\omega)$ show oscillatory behavior with Im $G(q,\omega)$ and Re $G(q,\omega)$ approaching, respectively, zero and a constant value at large ω. The oscillations are seen to grow with increasing r_s. Interestingly at $q/k_F=3.2$, Re $G(q,\omega)$ attains values greater than unity in the small ω region. In the instability region (i.e., $r_s>r_s^c$), the oscillations in the LFC factor get so pronounced that Re $G(q,\omega)$ exceeds unity at relatively large values of ω, as well. Consequently, the effective dynamic interaction potential, i.e., $\{V(q)[1-\text{Re } G(q,\omega)]\}$, becomes prominently attractive over certain ω intervals in the instability region. Qualitatively, similar behavior of $G(q,\omega)$ is found at other values of b. It may be added that the oscillatory trends in $G(q,\omega)$ are not specific to 1D but are also observed in higher dimensions.[25,40]

The $G(q,\omega)$ obtained above is used to calculate the dynamic structure factor $S(q,\omega)$ as

$$S(q,\omega)=-\frac{\hbar}{\pi}\text{Im }\chi(q,\omega). \tag{15}$$

$S(q,\omega)$ describes the density-fluctuation spectrum of the electron system and can be measured directly through x-ray

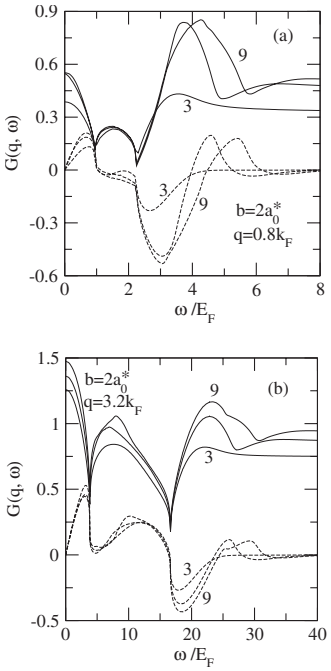

FIG. 13. The real (solid lines) and imaginary parts (dashed lines) of dynamic local-field correction factor $G(q,\omega)$ as a function of ω/E_F for $q/k_F=0.8$ [in panel (a)] and 3.2 [in panel (b)], for $r_s=3$, 7.5, and 9 at $b=2a_0^*$.

inelastic-scattering experiments. Although we have calculated $S(q,\omega)$ in the entire $q-\omega$ plane over a wide range of r_s and b values, we report here the results only at $b=0.1a_0^*$ in the density and wave-vector region where electron liquid shows instability with respect to the WC phase. Figure 14 depicts $S(q,\omega)$ as a function of ω/E_F (E_F is the Fermi energy) for $r_s=3$ at selected values of q/k_F (namely, 3.2, 3.4, 3.6, 3.8, and 4) including the one representing the period of density modulation ($q_c=3.6k_F$) of the WC phase. $S(q,\omega)$ starts exhibiting a broad peak in the small ω region at $q=3.2k_F$. Interestingly, this peak grows in magnitude and also shifts toward even smaller ω as q approaches q_c; for instance, the peak is located at $\omega/E_F\approx 0.05$ for $q=q_c$. Moreover, the peak in $S(q,\omega)$ becomes less pronounced and moves to higher ω values as one increases q beyond q_c. Although not shown in Fig. 14, changing r_s around three

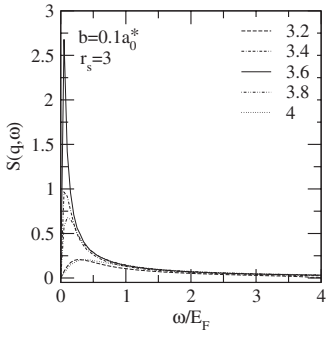

FIG. 14. Dynamic structure factor $S(q,\omega)$ (in units of inverse Fermi velocity) as a function of ω/E_F for $r_s=3$ at wire width $b=0.1a_0^*$. Legends denote the values of q/k_F.

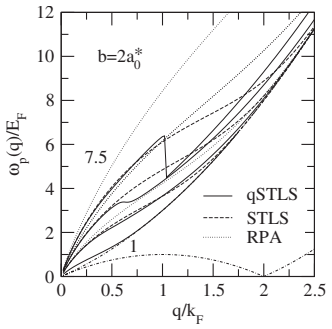

FIG. 15. Plasmon frequency $\omega_p(q)/E_F$ as a function of q/k_F at $b=2a_0^*$ in qSTLS ($r_s=1$, 3, 5, and 7.5), STLS, and RPA ($r_s=3$, 5, and 7.5). Legends indicate the values of r_s. The dash-dotted lines mark the boundary of electron-hole pair continuum.

results in suppression and broadening of the small ω peak at $q=3.6k_F$ in $S(q,\omega)$. These results of $S(q,\omega)$ suggest that it costs the electron system at $r_s=3$ negligibly small amounts of energy for excitation to the density-modulated state of wave vector q_c (i.e., the WC state). This seems to imply that the onset of the liquid-WC phase transition in the Q1D system may manifest in the form of a soft mode in the dynamic excitation spectrum. This mode might be observable experimentally as it lies well outside the electron-hole continuum.

Further, we wish to mention that $S(q,\omega)$ becomes negative in the qSTLS approach over a range of ω values (although not shown in Fig. 14), which obviously constitutes an unphysical result. With $S(q,\omega)$ being determined solely by the dynamic LFC factor, its negative values clearly indicate a flaw in the qSTLS dynamic LFC factor. A similar kind of observation has also been made by Tanatar and Bulutay.[27]

D. Plasmon excitation spectrum

The plasmon excitation spectrum in the qSTLS is obtained by the poles of dynamic density response function $\chi(q,\omega)$, i.e., from the zeros of the following equation

$$1-V(q)\{\chi_0'(q,\omega)[1-G'(q,\omega)]+\chi_0''(q,\omega)G''(q,\omega)\}=0. \tag{16}$$

Here, superscripts single and double prime stand, respectively, for the real and imaginary parts of the quantities involved. To find the plasmon excitation frequency $\omega_p(q)$, we solve the Eq. (16) numerically. However, a closed-form expression of $\omega_p(q)$ can be obtained in the STLS approximation because of the static nature of LFC factor. The numerical calculation of $\omega_p(q)$ reveals that the Eq. (16) has solution inside as well as above the electron-hole continuum. We emphasize that only the solution existing outside the continuum is important and corresponds to the collective mode while the one lying inside the continuum may not be experimentally observable, and hence, seems to have no physical significance. A similar result in 1D was also found using RPA by Das Sarma and Hwang.[17]

The numerical results for $\omega_p(q)$ in the qSTLS approach are depicted in Fig. 15 for $r_s=1$, 3, 5, and 7.5 at $b=2a_0^*$. We also report $\omega_p(q)$ in the STLS and RPA at the same wire

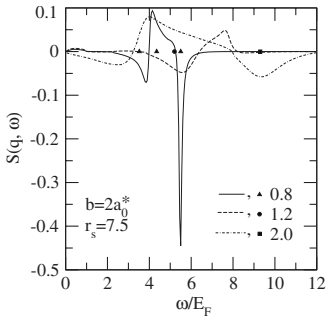

FIG. 16. Dynamic structure factor $S(q,\omega)$ (in units of inverse Fermi velocity) as a function of ω/E_F for $r_s=7.5$ at $b=2a_0^*$. Legends denote the values of q/k_F. Symbols correspond to the values of $\omega_p(q)$ as calculated by Eq. (16).

width for $r_s=3$, 5, and 7.5. At $r_s=1$, both the RPA and STLS curves are almost indistinguishable from the qSTLS results and, therefore, are not shown. The correction due to the inclusion of the dynamics of the LFC factor starts becoming visible with the increasing r_s and, in particular, the qSTLS $\omega_p(q)$ lie considerably below the RPA predictions. However, we find that the Eq. (16) starts exhibiting multiple roots for $r_s>6$ (in the region well above the electron-hole continuum) over a range of q values; for instance, there are three roots at $r_s=7.5$ in the q interval $0.6\leq q/k_F\leq 1$. Keeping in view the direct relationship between $\omega_p(q)$ and the location of peak in $S(q,\omega)$, we have plotted $S(q,\omega)$ in Fig. 16 at $r_s=7.5$ for $q/k_F=0.8$, 1.2 and 2. The corresponding roots of the Eq. (16) have also been depicted in the same figure by symbols. We note that, only for one root, there exists a well-defined peak in $S(q,\omega)$ at $q/k_F=0.8$, and this root is taken as $\omega_p(q)$ in Fig. 15. For $0.6>q/k_F>1$, where Eq. (16) possesses a single root, $\omega_p(q)$ coincides perfectly with the peak position in $S(q,\omega)$ for all q except for those in the interval $1<q/k_F<1.8$. The multiple roots of Eq. (16) and the apparent mismatch of $\omega_p(q)$ with the peak location in $S(q,\omega)$ over a range of q values for $r_s>6$ constitute a very unusual result, and it reflects in Fig. 15 as a sharp kink in the plasmon dispersion curve at $r_s=7.5$. One may also note from Fig. 16 that $S(q,\omega)$ assumes negative values (an unphysical result in itself) for certain ω intervals. We may add here that $S(q,\omega)$ shows negative behavior at the smaller r_s values also. These results obviously point to inadequacy of the qSTLS theory in describing the dynamical properties of the electron system.

Further, it is found that the curves of $\omega_p(q)$ merge with the electron-hole excitation region beyond a critical value of wave vector, which is found to decrease upon the inclusion of the LFC factor. In the qSTLS approximation, the value of this cut-off wave vector is slightly higher than its value when predicted by the STLS. Also, the cut-off wave vector is seen to increase with r_s. A similar behavior of $\omega_p(q)$ is found at other values of wire width, as well.

On the experimental side,[7] plasmon excitation spectrum has been studied at relatively higher values of electron density ($r_s\approx 1$) and wire width (i.e., in the weak correlation regime), and accordingly, even the RPA has been quite successful[41] in explaining the experimental data.

IV. SUMMARY AND CONCLUSIONS

The quantum version of the self-consistent mean-field approximation of Singwi *et al.*, which includes short-range correlations through a frequency and wave-vector dependent local-field correction factor, has been used to calculate the various static and dynamic properties of Q1D electron gas over a wide coupling regime. The static correlation functions and correlation energy have been compared directly with the LRDMC simulation data, and also, to the results of static mean-field theories and RPA. The comparative study reveals that the qSTLS approach captures reasonably well the qualitative behavior of the static correlation functions, as predicted by the LRDMC study, viz. the peaked structure in $S(q)$ or, equivalently, the periodic oscillations in $g(r)$. While these features of $S(q)$ and $g(r)$ are simply absent in the conventional STLS approach. In overall, the qSTLS results are found to compare more favorably with the LRDMC data. However, the extent of quantitative agreement of the qSTLS predictions becomes less in the strong-coupling regime, which reflects in the behavior of correlation energy, as well.

As an important finding, we have deduced that the difficulty in obtaining the self-consistent density response function $\chi(q,\omega)$ in the qSTLS approach at and beyond a critical r_s (i.e., r_s^c) is related to the emergence of an unphysical singularity in $\chi(q,\iota\omega)$. Although such a singularity implies the breakdown of the qSTLS approach for $r_s>r_s^c$, a purely mathematical scheme has been proposed to handle the singularity in order to have some insight into the mechanism, which leads to the eventual breakdown of the qSTLS theory. With this modification, we were able to generate the self-consistent $\chi(q,\omega)$ for r_s well above r_s^c. On the other hand, there is no such problem of singularity in $\chi(q,\omega)$ in the STLS approximation. Interestingly, at $r_s=r_s^c$, the static density susceptibility $\chi(q,0)$ has been found to diverge at a finite q value close to the reciprocal-lattice vector of 1D solid. The divergence in $\chi(q,0)$ has been interpreted as a precursor of Wigner crystallization in Q1D electron system. This structural instability also reflects in the behavior of other static, as well as dynamic, properties. Particularly, $S(q,\omega)$ is found to develop a sharp peak at nearly zero frequency for the q value at which $\chi(q,0)$ exhibits divergence. This seems to suggest that transition to the crystal phase may appear in the form of a soft mode in the dynamic excitation spectrum. However, the LRDMC study indicates only the possibility of a quasicrystalline phase in 1D, and therefore, the qSTLS prediction of Wigner crystallization seems to reflect the misrepresentation of correlation effects in the strong-coupling regime. This shortcoming of the qSTLS theory also manifests in the plasmon dispersion relation.

In conclusion, our study establishes firmly that it is crucial to include the dynamical character of correlations in describing the ground-state behavior of Q1DEG. At the same time, we have also observed that the qSTLS (as well as STLS) theory used by us is not that much successful in 1D as it is for the 3D and 2D electron systems. Interestingly, Asgari[42] has recently found that the Fermi hypernetted-chain approximation, which otherwise accounts quite accurately for the correlation effects in 2D and 3D, does not prove so in a 1D electron system. This clearly suggests that the electron cor-

relations are relatively much stronger in 1D as compared to higher dimensional situations. Therefore, there exists a need to have a more refined theory capable of dealing with strong correlations as manifesting in a Q1D electron system. It would be equally important to consider the Luttinger liquid description of the Q1DEG and have a direct comparison of the predictions thereof with the available LRDMC simulation data.

ACKNOWLEDGMENTS

One of us (K.K.) acknowledges the financial assistance provided by CSIR (New Delhi, India). We also thank G. Senatore and M. Casula for providing us their LRDMC simulation data.

APPENDIX A: $\chi_0(q,q',\omega)$ ON REAL AND IMAGINARY ω AXIS IN ONE DIMENSION

Performing the p integration in Eq. (4), the real and imaginary parts of $\chi_0(q,q',\omega)$ (at zero temperature) are obtained, respectively, as

$$\chi_0'(q,q',\omega) = \frac{m^*}{\pi q} \ln\left|\frac{\omega^2-\omega_-^2}{\omega^2-\omega_+^2}\right|, \tag{A1}$$

and

$$\chi_0''(q,q',\omega) = \begin{cases} -\dfrac{m^*}{q} & \text{for} \dfrac{qq'}{2m^*} > 0 \ \text{and} |\omega_-| < \omega < \omega_+ \\ \dfrac{m^*}{q} & \text{for} \dfrac{qq'}{2m^*} < 0 \ \text{and} |\omega_+| < \omega < \omega_- \\ 0 & \text{otherwise} \end{cases}, \tag{A2}$$

where $\omega_\pm = \frac{qk_F}{m^*} \pm \frac{qq'}{2m^*}$, are the boundaries of electron-hole pair continuum.

$\chi_0(q,q',\iota\omega)$ can be obtained directly from Eq. (A1) by substituting $\iota\omega$ for ω as

$$\chi_0(q,q',\iota\omega) = \frac{m^*}{\pi q} \ln\left|\frac{\omega^2+\omega_-^2}{\omega^2+\omega_+^2}\right|. \tag{A3}$$

APPENDIX B: MODIFICATION OF EQ. (10) DUE TO THE PRESENCE OF POLES IN $\chi(q,\iota\omega)$

In the instability region, $\chi(q,\omega)$ starts exhibiting a pole on the positive imaginary ω axis, say at $\iota\omega_0$, with ω_0 being real and positive. Following Landau and Lifshitz,[31] consider the contour integral as given by

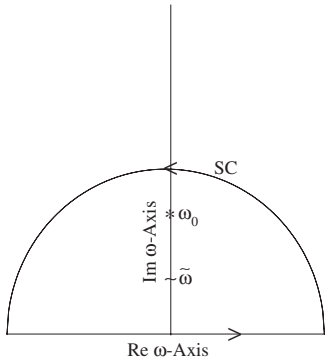

FIG. 17. Integration contour C in Eq. (B1). $\tilde{\omega}$ and ω_0 represent the poles of integrand in Eq. (B1).

$$\int_C dz \frac{z\chi(q,z)}{z^2+\tilde{\omega}^2} = \int_{SC} dz \frac{z\chi(q,z)}{z^2+\tilde{\omega}^2} + \int_{-\infty}^{\infty} d\omega \frac{\omega\chi(q,\omega)}{\omega^2+\tilde{\omega}^2}$$
$$= 2\pi\iota \sum [\text{Enclosed residues}]. \tag{B1}$$

As shown in Fig. 17, the contour C consists of a semicircle (SC) of infinite radius in the upper half of the complex ω plane. Evidently, the integrand in Eq. (B1) has poles at $z=\iota\tilde{\omega}$ and $\iota\omega_0$. Assuming the pole at $z=\iota\omega_0$ to be of first order, and by noting that the integration along the contour SC vanishes, Eq. (B1) is simplified as

$$\int_{-\infty}^{\infty} d\omega \frac{\omega\chi(q,\omega)}{\omega^2+\tilde{\omega}^2} = 2\pi\iota\left[\frac{\chi(q,\iota\tilde{\omega})}{2} + \frac{\iota\omega_0 a_{-1}}{\tilde{\omega}^2-\omega_0^2}\right], \tag{B2}$$

where

$$a_{-1} = \frac{\chi_0(q,\iota\omega_0)}{D'(q,\iota\omega_0)}, \tag{B3}$$

is the residue of $\chi(q,z)$ at $z=\iota\omega_0$ while $D'(q,\iota\omega_0)$ denotes the frequency derivative of the denominator of $\chi(q,z)$ at $z=\iota\omega_0$.

Using the property that $\chi'(q,\omega)=\chi'(q,-\omega)$ and $\chi''(q,\omega)=-\chi''(q,-\omega)$, and integrating the Eq. (B2) with respect to $\tilde{\omega}$, we have

$$\int_0^{\infty} d\omega\chi''(q,\omega) = \int_0^{\infty} d\omega\left[\chi(q,\iota\omega) - \frac{a_{-1}}{\omega-\omega_0} + \frac{a_{-1}}{\omega+\omega_0}\right], \tag{B4}$$

which provides the necessary modification of Eq. (10) due to pole on the positive imaginary axis.

*rkmoudgil13@gmail.com

[1] W. I. Friesen and B. Bergersen, J. Phys. C **13**, 6627 (1980).
[2] S. Das Sarma and Wu-Yan Lai, Phys. Rev. B **32**, 1401 (1985).
[3] A. Gold and A. Ghazali, Phys. Rev. B **41**, 7626 (1990).
[4] G. Y. Hu and R. F. O'Connell, Phys. Rev. B **42**, 1290 (1990).
[5] M. H. Degani and O. Hipólito, Surf. Sci. **229**, 279 (1990).
[6] W. Hansen, M. Horst, J. P. Kotthaus, U. Merkt, Ch. Sikorski, and K. Ploog, Phys. Rev. Lett. **58**, 2586 (1987).
[7] A. R. Goñi, A. Pinczuk, J. S. Weiner, J. M. Calleja, B. S. Dennis, L. N. Pfeiffer, and K. W. West, Phys. Rev. Lett. **67**, 3298

(1991).
[8] S. M. Cronenwett, H. J. Lynch, D. Goldhaber-Gordon, L. P. Kouwenhoven, C. M. Marcus, K. Hirose, N. S. Wingreen, and V. Umansky, Phys. Rev. Lett. **88**, 226805 (2002); D. J. Reilly, T. M. Buehler, J. L. O'Brien, A. R. Hamilton, A. S. Dzurak, R. G. Clark, B. E. Kane, L. N. Pfeiffer, and K. W. West, *ibid.* **89**, 246801 (2002).
[9] O. M. Auslaender, H. Steinberg, A. Yacoby, Y. Tserkovnyak, B. I. Halperin, K. W. Baldwin, L. N. Pfeiffer, and K. W. West, Science **308**, 88 (2005).
[10] H. Steinberg, O. M. Auslaender, A. Yacoby, J. Qian, G. A. Fiete, Y. Tserkovnyak, B. I. Halperin, K. W. Baldwin, L. N. Pfeiffer, and K. W. West, Phys. Rev. B **73**, 113307 (2006).
[11] O. M. Auslaender, A. Yacoby, R. de Picciotto, K. W. Baldwin, L. N. Pfeiffer, and K. W. West, Science **295**, 825 (2002).
[12] H. J. Schulz, Phys. Rev. Lett. **71**, 1864 (1993).
[13] J. M. Luttinger, J. Math. Phys. **4**, 1154 (1963); S. Tomonaga, Prog. Theor. Phys. **5**, 544 (1950).
[14] Ben Yu-Kuang Hu and S. Das Sarma, Phys. Rev. Lett. **68**, 1750 (1992); Ben Yu-Kuang Hu and S. Das Sarma Phys. Rev. B **48**, 5469 (1993); Also see, D. W. Wang, A. J. Millis, and S. Das Sarma, Phys. Rev. Lett. **85**, 4570 (2000), and references given therein.
[15] Michele Casula, Sandro Sorella, and Gaetano Senatore, Phys. Rev. B **74**, 245427 (2006).
[16] Q. P. Li and S. Das Sarma, Phys. Rev. B **43**, 11768 (1991).
[17] S. Das Sarma and E. H. Hwang, Phys. Rev. B **54**, 1936 (1996).
[18] L. Calmels and A. Gold, Solid State Commun. **92**, 619 (1994); Phys. Rev. B **52**, 10841 (1995).
[19] L. Calmels and A. Gold, Phys. Rev. B **56**, 1762 (1997).
[20] K. S. Singwi, M. P. Tosi, R. H. Land, and A. Sjölander, Phys. Rev. **176**, 589 (1968).
[21] L. Calmels and A. Gold, Phys. Rev. B **57**, 1436 (1998).
[22] Daniele Agosti, Francesco Pederiva, Enrico Lipparini, and Kazuo Takayanagi, Phys. Rev. B **57**, 14869 (1998).
[23] C. F. Richardson and N. W. Ashcroft, Phys. Rev. B **50**, 8170 (1994).
[24] D. Neilson, L. Świerkowski, A. Sjölander, and J. Szymański, Phys. Rev. B **44**, 6291 (1991).
[25] R. K. Moudgil, P. K. Ahluwalia, and K. N. Pathak, Phys. Rev. B **52**, 11945 (1995).
[26] T. Hasegawa and M. Shimizu, J. Phys. Soc. Jpn. **38**, 965 (1975).
[27] B. Tanatar and C. Bulutay, Phys. Rev. B **59**, 15019 (1999).
[28] E. Lieb and D. Mattis, Phys. Rev. **125**, 164 (1962).
[29] D. Pines and P. Noziers, *The Theory of Quantum Liquids* (Benjamin, New York, 1966), Vol. 1.
[30] See, for example, G. D. Mahan, *Many-Particle Physics*, 2nd ed. (Plenum, New York, 1990).
[31] See, for example, L. D. Landau and E. M. Lifshitz, *Statistical Physics*, 3rd ed. (Pergamon, New York, 1980), Pt. 1.
[32] B. Tanatar, I. Al-Hayek, and M. Tomak, Phys. Rev. B **58**, 9886 (1998).
[33] N. D. Mermin and H. Wagner, Phys. Rev. Lett. **17**, 1133 (1966).
[34] N. D. Mermin, Phys. Rev. **176**, 250 (1968).
[35] S. Nagano and K. S. Singwi, Phys. Rev. B **27**, 6732 (1983).
[36] K. S. Singwi and M. P. Tosi, Solid State Phys. **36**, 177 (1981); Krishan Kumar, Vinayak Garg, and R. K. Moudgil (unpublished).
[37] M. Jonson, J. Phys. C **9**, 3055 (1976); B. Tanatar and D. M. Ceperley, Phys. Rev. B **39**, 5005 (1989).
[38] T. M. Rice, Ann. Phys. (N.Y.) **31**, 100 (1965).
[39] H. J. Schulze, P. Schuck, and N. Van Giai, Phys. Rev. B **61**, 8026 (2000).
[40] A. Holas and S. Rahman, Phys. Rev. B **35**, 2720 (1987); Herwig K. Schweng and Helga M. Bohm, *ibid.* **48**, 2037 (1993).
[41] Q. P. Li, S. Das Sarma, and R. Joynt, Phys. Rev. B **45**, 13713 (1992).
[42] R. Asgari, Solid State Commun. **141**, 563 (2007).